Direct comparison of mechanical and optical measurements of the finish of precision machined optical surfaces

E. L. Church
U.S. Army Armament Research and Development Center
Dover, New Jersey 07801-5001

T. V. Vorburger
National Bureau of Standards
Gaithersburg, Maryland 20899

J. C. Wyant
Optical Sciences Center
University of Arizona
Tucson, Arizona 85721

Abstract. This paper compares two methods of measuring the finish of precision machined optical surfaces: the older, well-established mechanical stylus gauge and a recently developed optical gauge using interference microscopy. Results are found to be in good quantitative agreement for both random and periodic surface features, provided that appropriate filtering procedures are included in the data analysis to account for the differing transfer functions and bandwidths of the two measurement techniques. These results affirm the use of these techniques for the quantitative measurement and specification of machined optical surfaces.

Subject terms: surface metrology; precision machining; diamond turning; single-point machining; surface finish; profilometry; machined optics.

Optical Engineering 24(3), 388-395 (May/June 1985).

CONTENTS

1. INTRODUCTION

This paper discusses the analysis of surface profile measurements and compares mechanical and optical stylus measurements of two types of test surfaces. It confirms and extends the results of a paper on the same subject published previously.[1]

The mechanical stylus measurements were made using the digitized Talystep* at the National Bureau of Standards in Gaithersburg, Maryland.[2,3] This instrument measures the surface profile by drawing a fine diamond-tipped stylus across the surface and converting its vertical motion into an electrical signal by an electromechanical transducer. This is the same instrument used earlier,[1] except for cleaning of the lead screw and replacement of the stylus tip.

*Certain items of commercial equipment are identified in this paper to specify experimental procedures. In no case does such identification imply recognition or endorsement by the Department of Defense or the Department of Commerce.

Invited Paper ME-103 received Nov. 15, 1984; revised manuscript received Feb. 13, 1985; accepted for publication Feb. 15, 1985; received by Managing Editor Feb. 28, 1985. This paper is a revision of Paper 508-13 which was presented at the SPIE conference on Production Aspects of Single Point Machined Optics, Aug. 23-24, 1984, San Diego, CA. The paper presented there appears (unrefereed) in SPIE Proceedings Vol. 508.

The optical stylus measurements were made using a Wyko model 1000 noncontacting profiling microscope.[4] This instrument measures the surface profile by determining the phase variations of the light reflected normally from the surface and converting them into height variations using

$$Z(x) = \frac{\lambda}{4\pi}\,\phi(x)\ , \qquad (1)$$

where $\lambda = 0.6328\ \mu m$ is the mean measuring wavelength. As previously,[1] measurements were made at Wyko Optical, Inc. (Tucson, Arizona) using a stock instrument with a 20× objective.

Raw profile data from each measurement were recorded and analyzed at Brookhaven National Laboratory (Upton, New York) using routines developed under the aegis of the National Synchrotron Light Source.[1,5,6] Results are discussed here in terms of two profile statistics: the power spectral density and bandwidth-limited values of the root-mean-square (rms) roughness. These were chosen because of their direct relationship with functional performance of the surfaces when used in an optical system. The first is a one-to-one mapping of the scattered-light intensity, and the second is directly related to the total integrated scatter (TIS) or Strehl factor.[5,7]

The test surfaces, germanium and silicon disks supplied by Pneumo Precision, Inc. (Keene, New Hampshire), were nominally flat, finished by single-point fly cutting. Machined surfaces were chosen because they exhibit both random and periodic features and because profile data taken across the lay of such surfaces are more directly interpreted than those of polished surfaces.[5-8]

The surfaces used had finishes of the order of 50 to 100 Å, chosen to fall comfortably within the measurement ranges of the instruments rather than to represent the state of the art of finishing. A discussion of state-of-the-art surfaces is given in another paper in this collection.[9] Although the two sets of test surfaces were machined under similar conditions, their surface textures were very different: the finish of the germanium was mainly in the form of low-frequency random roughness while the silicon showed high-frequency periodic

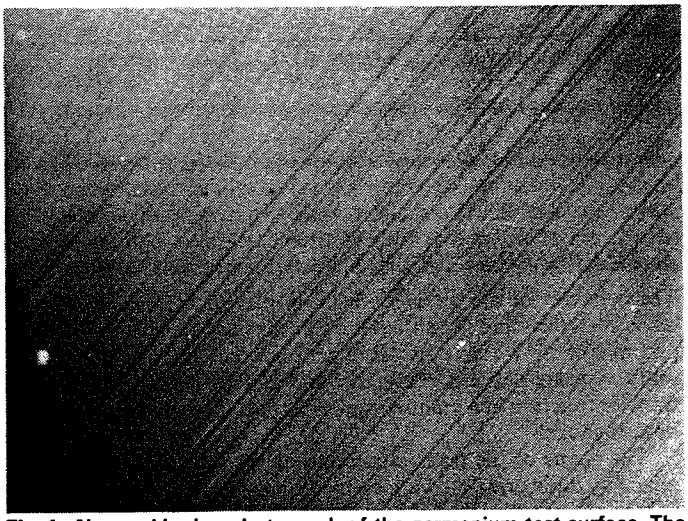

Fig. 1. Nomarski microphotograph of the germanium test surface. The long dimension in the photograph is 240 μm.

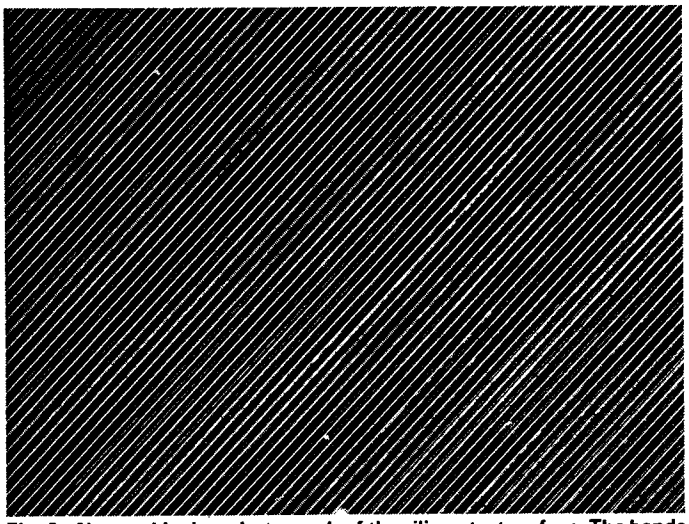

Fig. 2. Nomarski microphotograph of the silicon test surface. The bands correspond to the 3.4 μm tool feed.

roughness. As discussed below, this complementarity provides a sensitive test of our understanding of the measurement process.

Figures 1 and 2 are Nomarski microphotographs of the germanium and silicon surfaces, respectively. The tool marks on the germanium surface are fairly random, while the striking bands in the photograph of the silicon surface clearly show the 3.4 μm tool-feed spacing. These differences in texture are also very conspicuous to the eye: the germanium appears smooth, while the silicon appears rough and displays diffraction colors.

2. LINEAR MEASUREMENTS

The measurement process may be viewed as a mathematical operation:

$$Z_{\text{measured}} = MZ_{\text{object}} , \tag{2}$$

where M is a measurement operator and Z, in our case, is the surface profile. A good measurement is one for which M is in the unit operation over as wide an operating range as possible.

The most desirable measurements are linear; that is, sine waves are measured with no harmonic distortion. In that case, Eq. (2) takes the form of a convolution in real space:

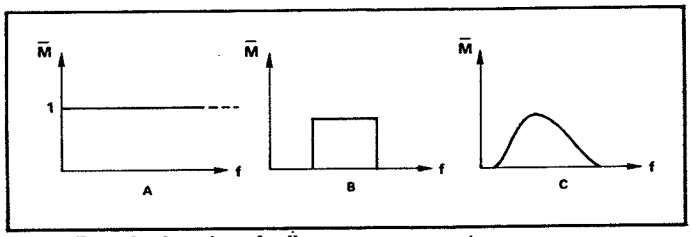

Fig. 3. Transfer functions for linear measurements.

$$Z_{\text{measured}}(x) = M(x) * Z_{\text{object}}(x) , \tag{3}$$

or, equivalently, a simple multiplication in frequency space:

$$\bar{Z}_{\text{measured}}(f) = \bar{M}(f)\bar{Z}_{\text{object}}(f) , \tag{4}$$

where the overbar denotes the Fourier transform. M(x) is then the measurement impulse response, and $\bar{M}(f)$ is its transfer function. Because of the simple multiplicative form of Eq. (4), it is convenient to compare measurement systems in the frequency domain.

We take the mechanical gauge to behave as a linear measuring instrument over its operating range as defined in the following section. The optical gauge may be shown to behave as a linear instrument in the smooth-surface limit

$$\left(\frac{4\pi Z_{\text{rms}}}{\lambda}\right)^2 \ll 1 , \tag{5}$$

where Z_{rms} is the root-mean-square roughness. Details will be published elsewhere.

Figure 3 is a sketch of canonical forms of measurement transfer functions. The perfect curve, A, is unity for all frequencies—a practical impossibility. Curve B is the ideal curve—unity over as wide a range as possible and zero outside. Curve C is a realistic curve—the measurement is sensitive to a more-or-less well-defined range of frequencies with a frequency-dependent transfer function. Curve C can be transformed into a practical approximation of curve B by careful hardware design or, as discussed below, by processing the measurement data in subsequent software.

The ideal measurement situation would occur when the frequency content of the object being measured falls completely within the bandpass of the measurement apparatus, in which case the measurement result would be transparent to the technique used. In the case of surface roughness, the opposite situation holds: the roughness is spread over a wide range of surface wavelengths—from atomic diameters to the diameter of the workpiece—wider than the bandpass of any single measurement technique. In that case, the comparison and interpretation of measurements must necessarily take into account their differing transfer functions.

The following section discusses the bandwidth limits of the two instruments used here, and following that, the forms of their transfer functions.

3. EXTREME AND EFFECTIVE BANDWIDTH LIMITS

The bandwidth limits of profile measurements are determined by the total trace length and the sampling interval. If the trace length L is sampled at N equally spaced points, the extreme surface frequencies included in the measurement are

$$f_{\text{min}}^{(\text{extreme})} = \frac{1}{L} , \qquad f_{\text{max}}^{(\text{extreme})} = f_{\text{Nyquist}} = \frac{N}{2L} . \tag{6}$$

The effective values lie within these limits by amounts that depend on

TABLE I. Measurement Parameters*

Instrument	Number of Sampled Points N	Total trace length L	Sampling interval L/N	Effective $1/f_{max}$ 4L/N	Effective $1/f_{min}$ L/2
Mechanical	4000	1500	0.375	1.5	750
Optical	1024	665	0.649	2.6	333

*All distances in micrometers

details of the measurement process.

The effective low-frequency cutoff is determined by the fact that the raw profile data must be detrended to remove spurious piston (constant), tilt (linear), and possibly power (quadratic) contributions introduced during the measurement process. This is usually done by subtracting a least-squares polynomial fitted to each data set. It can be shown[1] that this operation is equivalent to a high-pass filtering operation that eliminates the frequency $f = 0$ and attenuates the frequency $f = 1/L$, but passes higher frequencies essentially unaffected. For this reason, we choose the effective low-frequency limit to be twice the extreme value given in Eq. (6).

The effective high-frequency limit is determined by the fact that any signal lying above the Nyquist frequency [Eq. (6)] is not eliminated, but appears as an alias within the measurement range at the frequency

$$f_{alias} = 2f_{Nyquist} - f \, . \tag{7}$$

Well-designed measurement systems include an antialiasing filter to attenuate or eliminate frequencies above the Nyquist frequency before the sampling operation in order to eliminate such effects. It is the properties of these antialiasing mechanisms that determine the effective upper frequency limit.

In the case of the mechanical gauge, antialiasing filtering is accomplished by the electrical and mechanical properties of the stylus instrument. Its transfer function has been measured[5] and was found to follow closely that of a simple low-pass filter:

$$\bar{M}(f) = \frac{1}{1 + (fd_o)^2} \, . \tag{8}$$

The value of d_o, the spatial wavelength for 50% amplitude attenuation, is 0.862 μm. The finite size of the stylus tip also attenuates the measurement of short surface wavelengths but does not place a significant limitation on the present study since its measured width is only of the order of 0.5 μm. In particular, the estimated tip curvature is significantly greater than the rms curvature of the test surfaces obtained by evaluating the fourth moments of their profile power spectra. The procedure for evaluating the latter is discussed in Ref. 1.

In the case of the optical gauge, antialiasing is accomplished by the finite resolving power of its optical microscope and the sampling aperture of the photodiode array in its focal plane, as discussed in the following section.

To stay within the bandwidth limits imposed by the various filtering operations, we take the effective range of surface frequencies to lie a factor of two within the extreme values given in Eq. (6); that is

$$f^{(effect)}_{min} = \frac{2}{L} \, , \qquad f^{(effect)}_{max} = \frac{1}{2} f_{Nyquist} = \frac{N}{4L} \, . \tag{9}$$

Numerical values of these frequencies and other parameters of the measurements discussed below are given in Table I. These show that although the bandwidth limits of the two measurement techniques are different, so that raw measurements are not directly comparable, there is a considerable region of overlap over which quantitative comparisons can be made.

4. TRANSFER FUNCTIONS

The behavior of the transfer function of the mechanical measurement at its low- and high-frequency limits has been discussed above and in Ref. 5. We take its value between the effective limits to be unity. A more detailed analysis would include effects of a variable transfer function in a manner similar to that discussed below for the optical gauge.

The shape of the transer function of the optical gauge is determined by three principal factors: the finite temporal coherence of the light used, the properties of its optical system, and the finite pixel size of the photodiode array in its focal plane. The total transfer function of the measurement is then the product of three factors:

$$\bar{M}(f) = \bar{M}_{coherence} \bar{M}_{optics} \bar{M}_{array} \, . \tag{10}$$

We now examine these factors individually.

The instrument uses finite bandwidth light to eliminate interference effects: $\lambda = 0.6328 \pm 0.0200$ μm. The parameter describing the contrast attenuation due to a wavelength spread of $\Delta\lambda$ about λ is

$$\frac{\Delta\lambda}{\lambda} 4\pi \frac{Z_{rms}}{\lambda} \, . \tag{11}$$

However, the surfaces considered here satisfy the Rayleigh smoothness condition, Eq. (5), in which case coherence effects are negligible. That is, for our measurements

$$\bar{M}_{coherence}(f) = 1 \, . \tag{12}$$

The phase-to-intensity transfer function of the optical system depends on optical and structural details that are not readily accessible. For the present purposes, we model this as a simple triangle function:

$$\bar{M}_{optics}(f) = 1 - fd_{resol} \, , \tag{13}$$

where

$$d_{resol} = \frac{4}{\pi} \frac{\lambda}{2NA} \tag{14}$$

and NA is the numerical aperture of the objective. For the 20× objective used in the present measurements, NA = 0.4, from which it follows that $d_{resol} = 1$ μm. Equation (13) is simply the textbook form of the intensity-to-intensity modulation transfer function of a simple lens linearized by extrapolating its tangent at zero frequency, which accounts for the factor of $4/\pi$. An obvious refinement would be to use the full algebraic form appropriate for the annular aperture[10] resulting from the presence of the reference mirror in the microscope objective.

Each pixel of the photodiode array in the optical gauge integrates the intensity of the image over an essentially square aperture with a side length of approximately $L/N = 0.65$ μm when projected onto the surface being measured. In the instrument used here each measurement point corresponds to the average of two adjacent pixels. The resulting array transfer function is then

$$\bar{M}_{array}(f) = \frac{\sin(2\pi fL/N)}{2\pi fL/N} . \quad (15)$$

This function is unity at low frequencies and goes through its first zero at the Nyquist frequency of the array.*

At the effective high-frequency limit (Table I), the three amplitude-transfer-function factors in Eq. (10) have the values 1, 0.615, and 0.637, respectively, giving a total attenuation of 0.392. At the surface wavelength of 3.4 μm—the period of the tool marks in Fig. 2—the corresponding factors are 1, 0.706, and 0.777, giving a total attenuation of 0.548. Attenuations of this magnitude require correction.

To compensate for the nonconstant transfer function of the optical gauge, we include a restoration filter in the data analysis that consists of the frequency-domain inverse filter

$$\bar{M}_{inverse}(f) = \bar{M}^{-1}_{optics}(f)\bar{M}^{-1}_{array}(f) . \quad (16)$$

In principle, this filter can be used at frequencies above the effective maximum given in Table I. However, it diverges at the extreme frequency [Eq. (6)], which corresponds to a surface wavelength of 1.3 μm, and as a practical matter, we cut it off at 2 μm to avoid spurious noise effects. At that point the total amplitude restoration factor is 4.575, corresponding to a power restoration factor of 20.93.

5. DATA PROCESSING

Raw data from each instrument are first detrended by subtracting a least-squares quadratic fitted to the individual data sets. The detrended profiles (residuals) are then plotted to give the unrestored finish profile. These profiles are then passed through the restoration filter, which involves Fourier transformation using the FFT algorithm, multiplication by the restoration filter, and inverse transformation. The resulting restored profiles are also plotted.

In the mechanical case, the restoration filter involves simple multiplications by unity, and the restored and unrestored profiles are identical. In the optical case, restoration involves multiplication by the inverse filter in Eqs. (13) through (16) for frequencies up to 0.5 μm^{-1} and by zero for higher frequencies.

The restored residuals are then multiplied by a Hamming data window and the periodogram spectral estimate is formed by computing the square magnitude of the Fourier transform of the product. This spectrum is then plotted over the extreme range of surface frequencies spanned by the measurement technique involved.

Bandwidth-limited estimates of the rms surface roughness, slope, and curvature are then computed by evaluating weighted integrals (sums) of the spectrum over selected ranges of surface frequency. It is the comparison of these quantities, measured over the same ranges for each instrument, that offers the most sensitive test of the equivalence of the different measurement techniques.

The mathematical expressions for the operations described above are given in Ref. 1.

6. RESULTS FOR THE GERMANIUM SURFACES

Figures 4 and 5 show the raw and restored optical profiles of the germanium test surface shown in Fig. 1. Only the first 500 μm (0.5 mm) section of the profile is shown, although the full range of 665 μm was used in the analysis. The vertical scale corresponds to ±600 Å. The two profiles are essentially identical, although close examination shows that the restored profile does have greater fine structure.

Figure 6 is a section of a mechanical profile of the same surface plotted on the same scale as in Figs. 4 and 5. Although a one-to-one comparison with the preceding profiles is impossible since they were taken at different points on the surface, it is clear that there is a strong "statistical" similarity between the mechanical and optical data. In detail, however, the mechanical profile appears to show even greater fine structure than does the restored optical profile.

The proper way to appreciate these differences is to see how the roughness "power" is the distributed among different surface frequencies, that is, by looking at the spectral distributions of the profiles.

Figures 7, 8, and 9 are log-log plots of the periodograms of the three profiles shown in Figs. 4, 5, and 6, respectively. The vertical scale runs between 10^{-7} and 10^{-1} μm^{+3} (6 decades), and the horizontal frequency scale runs from 10^{-3} to 2 μm^{-1} (3+ decades). These

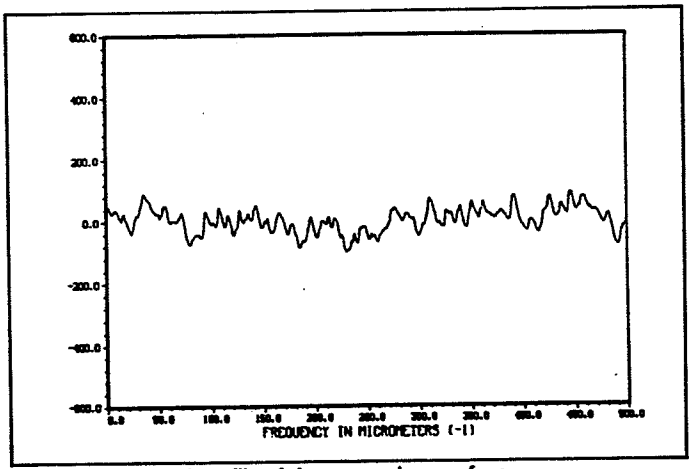

Fig. 4. Raw optical profile of the germanium surface.

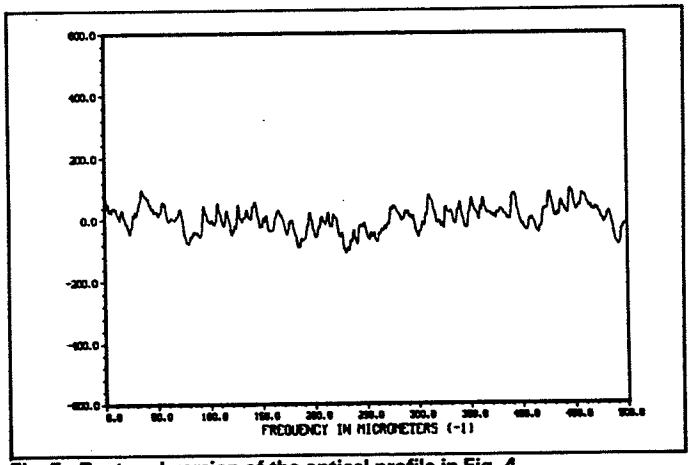

Fig. 5. Restored version of the optical profile in Fig. 4.

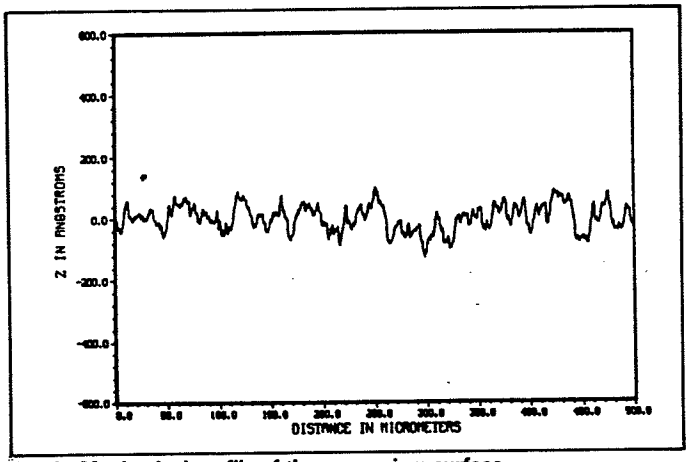

Fig. 6. Mechanical profile of the germanium surface.

*Equation (15) differs from Eq. (14) in Ref. 1 by the presence of the aspect ratio of 2 in the argument of the sinc function to account for the two-pixel averaging mentioned above.

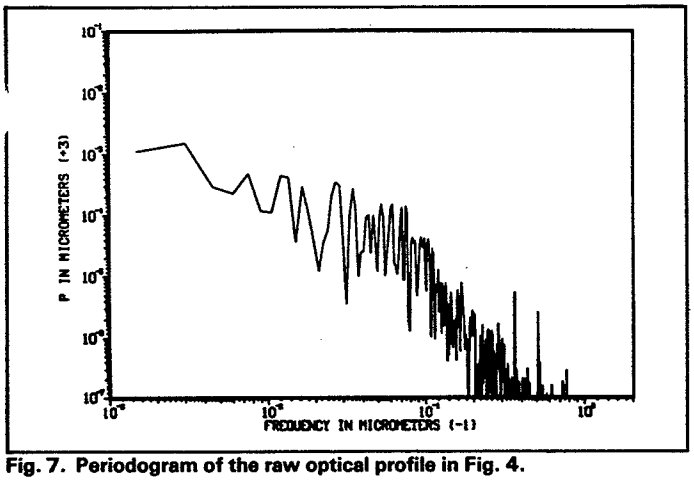

Fig. 7. Periodogram of the raw optical profile in Fig. 4.

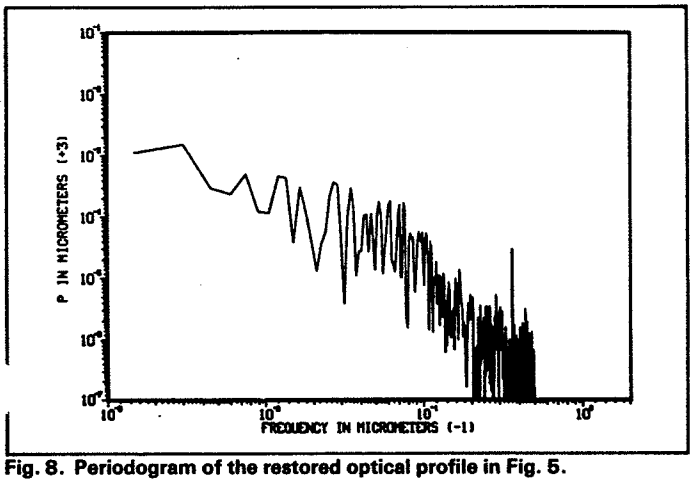

Fig. 8. Periodogram of the restored optical profile in Fig. 5.

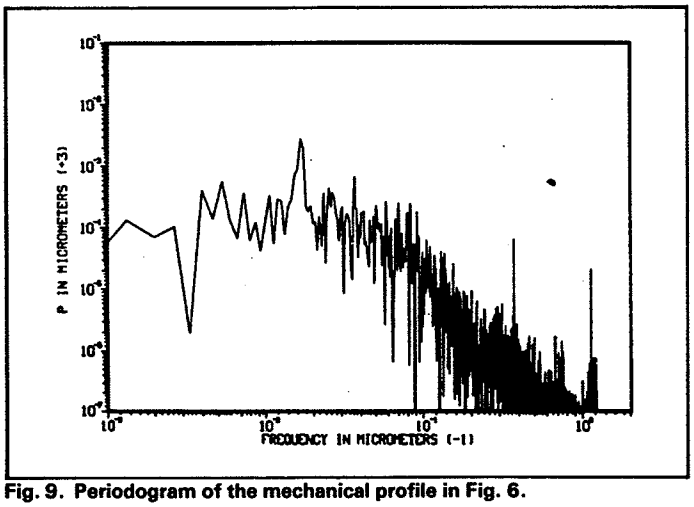

Fig. 9. Periodogram of the mechanical profile in Fig. 6.

wide ranges are required to display the full character of the structure found in these surfaces.

The three spectra are very similar except at high frequencies, which, in the germanium sample, represent only a small fraction of its total roughness. Figures 7 and 8 show the important amplification effects of the restoration filter at short wavelengths and its ultimate cutoff at 2 μm. The mechanical data, which extend to a wavelength of 0.75 μm, are clearly in better agreement with the restored than with the unrestored optical data over common frequency ranges.

The spectral lines at a wavelength of about 3 μm that appear in each spectrum are the fundamental of the tool marks' periodicity, which is hard to discern in the Nomarski microphotograph and is unrecognizable in the surface profiles. These spectral lines are of the order of two or three frequency bins wide, the natural linewidth for the Hamming data window. The additional lines at 1.9 μm in the optical spectrum and at 0.9 μm in the mechanical spectrum are taken to be spurious since they do not appear in other profiles of the same surface.

7. RESULTS FOR THE SILICON SURFACE

Figures 10 and 11 show the raw and restored optical profiles of the silicon surface shown in Fig. 2. In this case, only the first 100 μm section of the profile is shown, although again the full 665 μm of data were used in the analysis. The vertical scales are again ± 600 Å.

The conspicuous periodicities in the profiles correspond to the approximately 3 μm tool feed. However, there are two obvious differences in the profiles: the restored version has a larger amplitude, and the shape of the oscillations is smoother. In particular, the notch that frequently appears on the leading edges of the peaks in the unrestored profile is missing in the restored version.

Figure 12 is a mechanical profile of the same surface plotted on the same scales. Superficially, it is very different from either of the optical profiles; it has a much larger peak-to-valley distance, the peaks and valleys are sharper, and a distinct intermediate peak appears between the major ones. To appreciate the source of these differences, we examine the spectra of these profiles.

Figures 13, 14, and 15 are the periodograms of the profiles shown in Figs. 10, 11, and 12, respectively, on the same scales as the earlier spectra.

Figure 13 shows a pair of very sharp and intense lines that are the fundamental and first harmonic of the 3 μm tool feed. In Fig. 14, the first harmonic is cut off by the 2 μm cutoff of the restoration filter, leaving only the fundamental. This accounts for the simlutaneous amplification and smoothing of the shape of the oscillations in Fig. 11. It does not appear as a smooth sinusoid in Fig. 11 because the plotting routine uses a linear rather than a Whittaker interpolation scheme for connecting the discrete data points.

The mechanical data, Fig. 15, show the intense fundamental and the first harmonic of the tool feed, as well as the second and third harmonics. It is the presence of these higher harmonics in the mechanical measurements that lead to the greater amplitude and detail of the profile in Fig. 12.

The peaks of the mechanical lines are of the order of two to four frequency bins wide, which is again comparable with the natural Hamming width. However, they have considerably broader bases than do the optical lines, due, presumably, to the fact that the mechanical measurements involve a dynamic measurement system, which is subject to vibration and drive-rate fluctuations.

Comparison of the three spectra over common frequency ranges shows clearly that the restored optical spectrum is in much better agreement with the mechanical data than is its unrestored version.

8. QUANTITATIVE FINISH PARAMETERS

Surface profiles and spectra provide valuable complementary views of surface topography. Profiles can reveal extraneous spikes or pits in the measurement that would be difficult to recognize in the frequency domain. On the other hand, spectra can reveal small periodicities that are invisible in the profile tracings. These representations, however, are primarily visual and quantitative. A quantitative comparison can be made by examining finish parameters evaluated from the profile spectra over the same ranges of surface frequencies.

Table II lists a number of such parameters derived from the present series of measurements. Three types of measurements of three surfaces are compared (top to bottom): unrestored optical, restored optical, and mechanical measurements of two germanium surfaces and one silicon surface.

The parameters compared (left to right) are the period of the tool

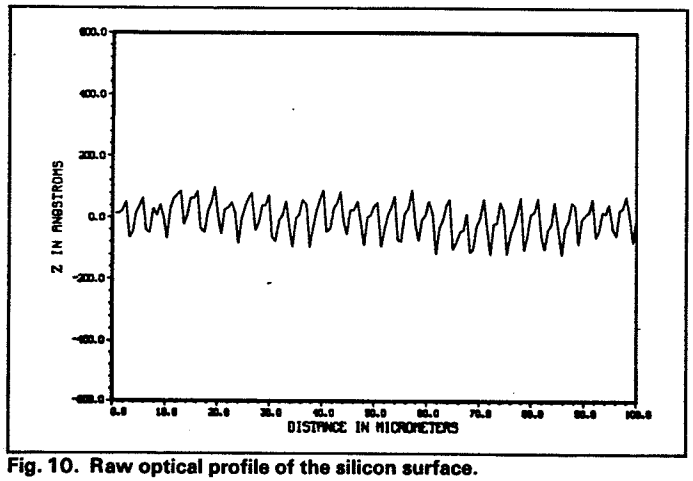

Fig. 10. Raw optical profile of the silicon surface.

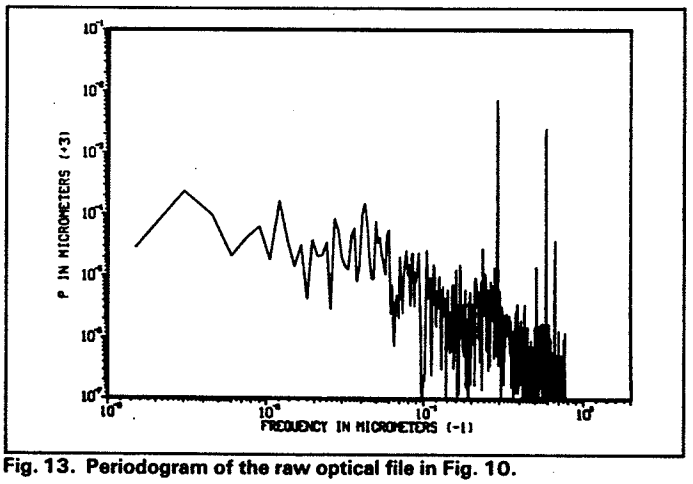

Fig. 13. Periodogram of the raw optical file in Fig. 10.

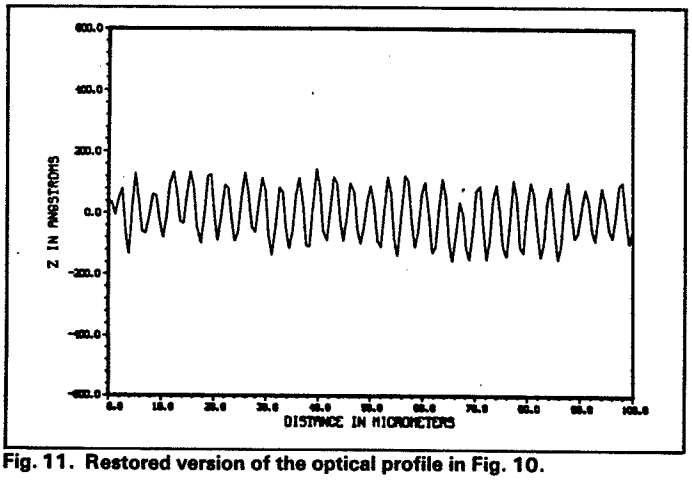

Fig. 11. Restored version of the optical profile in Fig. 10.

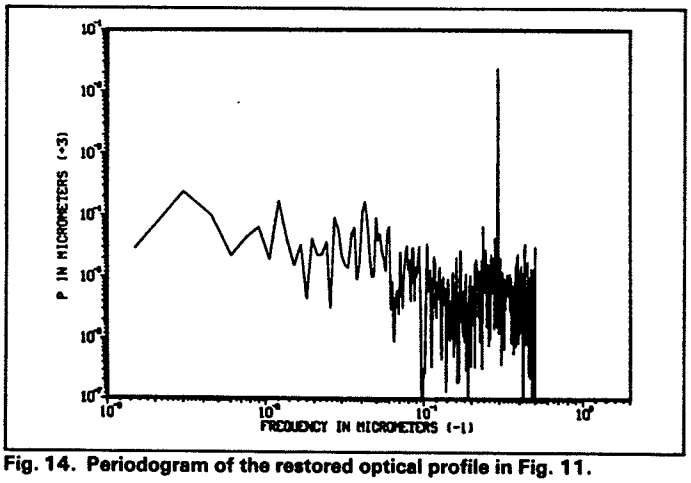

Fig. 14. Periodogram of the restored optical profile in Fig. 11.

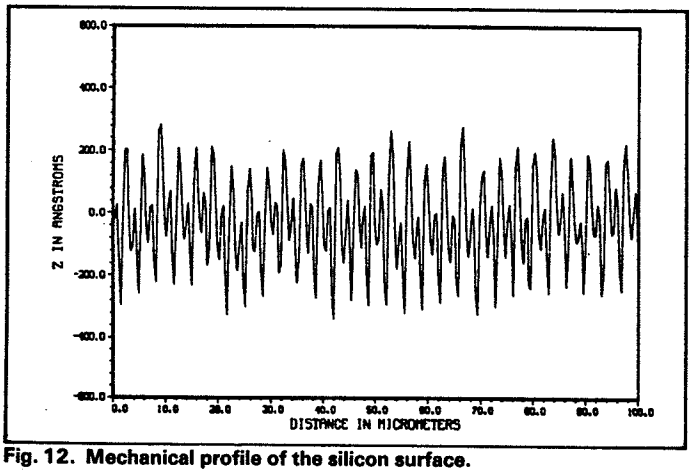

Fig. 12. Mechanical profile of the silicon surface.

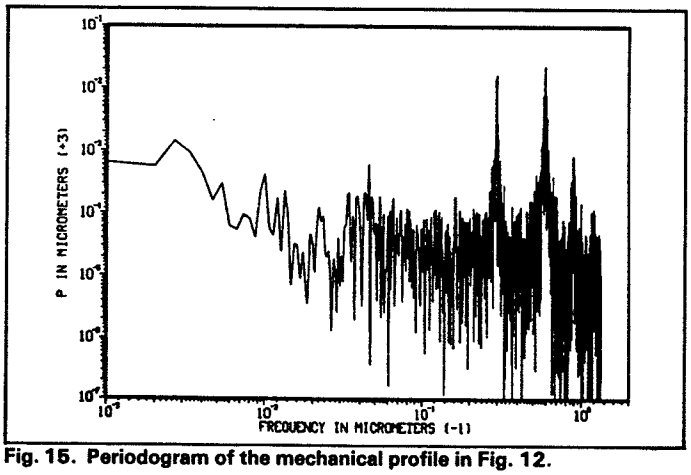

Fig. 15. Periodogram of the mechanical profile in Fig. 12.

marks, the amplitude of their fundamentals, and the rms values of the surface roughness obtained by integrating the spectral estimates between the indicated ranges of surface wavelengths: 2 to 12 μm, 12 to 333 μm, and 2 to 333 μm. The 2 μm limit is the cutoff of the optical restoration filter, 12 μm is the nominal upper limit of conventional TIS measurements made with normal-incidence HeNe light, and 333 μm is the effective upper wavelength limit imposed by the quadratic detrending of the optical data.

The last column of Table II gives the wide-open rms roughness values, that is, the nonequivalent values obtained by analysis of the unwindowed profile data over the extreme range of surface frequencies determined by the measurement procedures themselves (cf. Table I). The numbers in parentheses in the mode column are the numbers of independent measurements used to generate the average values and standard deviations given in the table.

9. DISCUSSION

The optical and mechanical measurements of the 3 μm tool feed are in excellent agreement for each sample, although there are significant

TABLE II. Finish Parameters

Mode	Line position μm	Amplitude fundamental Å	rms (f^{-1}=2–12 μm) Å	rms (f^{-1}=12–333 μm) Å	rms (f^{-1}=2–333 μm) Å	rms wide open Å
			GERMANIUM SURFACE #1			
Raw optical (6)	2.759±0.008	1.2± 0.1	10.3± 0.8	32.1± 3.0	33.7± 2.7	35.4± 2.8
Restored optical (6)	2.759±0.008	2.7± 0.2	12.8± 0.8	33.1± 3.0	35.5± 2.6	36.4± 2.8
Mechanical (2)	2.703±0.002	2.6± 0.1	13.7± 0.3	34.0± 3.4	36.7± 3.3	37.4± 3.0
			GERMANIUM SURFACE #2			
Raw optical (6)	3.035±0.021	1.9± 0.1	8.4± 0.9	36.3± 3.7	37.3± 3.6	38.1± 2.6
Restored optical (6)	3.035±0.021	3.8± 0.2	11.0± 1.0	37.3± 3.8	38.9± 3.7	39.3± 3.6
Mechanical (1)	2.977	4.1	10.6	34.7	36.3	37.8
			SILICON SURFACE			
Raw optical (2)	3.402±0.021	37.4± 4.4	39.2± 4.0	20.7± 3.5	44.6± 1.9	51.1± 0.7
Restored optical (2)	3.402±0.021	68.1± 7.6	70.8± 7.0	21.3± 3.4	74.1± 5.8	74.2± 5.7
Mechanical (3)	3.345±0.035	75.1±11.0	84.1±11.6	25.8± 0.5	88.0±11.0	145.7±14.0

surface-to-surface variations. The 3 Å amplitudes of the fundamental on the germanium surface are also in very good agreement after restoration, and are comparable with the value of 2 Å computed from the tool radius. It is noteworthy that this periodic surface feature with atomic dimensions is observed with a signal-to-noise ratio of roughly 50 to 1.

The various bandwidth-limited roughness values of the germanium surfaces, including the wide-open values in the last column, are in good agreement with or without restoration since the finish of these surfaces is dominated by long surface wavelengths. Results for the silicon surface, however, are quite different: restoration is essential to get agreement for the high-frequency (2 to 12 μm) and broadband (2 to 333 μm) values since these are dominated by the high-frequency tool marks.

The importance of comparing results over equal frequency ranges shown dramatically in the last column of the silicon data. Restoration is important, but even so, the mechanical roughness is still twice the optical value. The source of this difference lies not in the measurement techniques, but in the "apples-and-oranges" comparison of data involving different bandwidths.

10. SUMMARY AND CONCLUSIONS

This paper discusses surface profile measurements in general, mechanical and optical measurements in particular, and compares results obtained with two types of test surfaces: one dominated by low-frequency random roughness and the other by high-frequency periodic roughness.

The comparison is made over that overlapping region of frequency-amplitude space in which both measurement techniques are linear and have a common bandpass. The mechanical measurement is taken to have a constant transfer function over its effective bandwidth, while the optical measurement involves a nonconstant response that attenuates high surface frequencies. To compensate for this, a first-order model of the transfer function of the optical instrument is used to design a simple restoration filter that has been implemented in software compatible with the commercial instrument.

Qualitative and quantitative comparisons show the importance of restoration effects for broadband measurements of surfaces containing significant high-frequency roughness, for the study of tool marks, and for the extraction of finish information corresponding to large-angle surface scattering.

The agreement between the results of mechanical and optical measurements—one sensitive to mechanical properties at immense pressure and the other to electromagnetic properties at optical frequencies—is extremely gratifying, and affirms the use of these techniques for the quantitative measurement and specification of machined optical surfaces.

Appendix A discusses the effects of surface layers in the optical measurements, and Appendix B addresses the effects of surface rotation on linear profile measurements.

11. ACKNOWLEDGMENTS

The test surfaces were provided by R. Clark at Pneumo Precision, Inc. C. Giauque assisted with the Talystep measurements at the National Bureau of Standards, and C. Koliopoulos and S. Lange made the optical measurements at Wyko, Inc. At Brookhaven National Laboratory, P. Takacs provided valuable assistance and discussions, H. Berry carried through the data analyses, and W. Marin, Jr. prepared the Nomarski microphotographs. D. Aspnes at Bell Communications Research, Inc. provided information on surface layers. This work was suppported in part by the Department of Energy (E.L.C.) and the Department of Commerce (T.V.V.).

12. APPENDIX A: EFFECTS OF SURFACE LAYERS

The optical gauge measures the phase of the light reflected from the surface being examined. To convert phase into height we require a model. Eq. (1) is based on the model that the surface is a simple interface: air above and material below.

Real surfaces invariably involve some sort of chemical or physical layers deposited during or after the machining process. In interpreting the present measurements in terms of Eq. (1) we have made the implicit assumption that the effects of these layers are negligible. To justify this we examine a slightly more complicated physical model: a simple one-layer structure.

The addition of a layer of thickness t to a bare substrate shifts its apparent height, as determined by Eq. (1), according to

$$Z_{\text{layered}} = Z_{\text{bare}} + \frac{\lambda}{4\pi}\psi(t) , \tag{17}$$

where $\psi(t)$ is the phase of

$$Q = \frac{r_{01} + r_{12}\exp(-iq_l)}{1 + r_{01}r_{12}\exp(-iq_l)} \frac{\exp(+iq_a)}{r_{02}} . \tag{18}$$

Here

$$q_a \triangleq \frac{4\pi}{\lambda} N_a t , \tag{19}$$

and

$$r_{ab} = \frac{N_b - N_a}{N_b + N_a} \tag{20}$$

is the normal-incidence amplitude reflection coefficient of the a to b

interface, where the subscripts are 0 = air, 1 = layer, and 2 = substrate.

In the thin-film limit, $q \ll 1$,

$$Q = 1 + i4\pi \frac{t}{\lambda} \frac{1 - N_1^{-2}}{1 - N_2^{-2}} + \ldots . \tag{21}$$

If the indices of refraction N are real,

$$Z_{\text{layered}}(x) = Z_{\text{bare}}(x) + \frac{1 - N_1^{-2}}{1 - N_2^{-2}} t(x) + \ldots , \tag{22}$$

where, for simplicity, we have taken the index of air to be unity.

Surface layers on germanium and silicon consist of about 25 Å of oxide plus a layer of organic material with $N \sim 1.5$ whose thickness varies from essentially zero after cleaning to something of the order of another 25 Å after storage and handling. Substituting reasonable values for the various indices into Eq. (21), we find that the coefficient multiplying t(x) lies between 0.6 and 0.8. It follows that the magnitude of the layer contribution to the apparent optical height could amount to 15 to 40 Å, which is a significant amount.

The analogous expression for mechanical measurements obviously depends on the mechanical rather than on the optical properties of the layer. If we write

$$Z_{\text{layered}}(x) = Z_{\text{bare}}(x) + kt(x) + \ldots , \tag{23}$$

there are two obvious extemes: k = 1 for a "hard" layer and k = 0 for a completely "soft" one.

The critical quantity is not the total magnitude of the layer corrections in either Eqs. (22) or (23) but the magnitude of their fluctuations along the profile and their correlation with the height fluctuations of the substrate. A constant layer thickness, for example, would simply shift the apparent substrate profile by a constant amount, which would be unobservable either optically or mechanically.

The good agreement between the optical and mechanical measurements observed in the present experiments is attributed to the fact that over the surface-wavelength region explored, the layer tracks the substrate, and any differential effect is small and submerged in the experimental error.

However, as measurement accuracy improves and finer and finer interpretations of measurement data are attempted, one must be alert to the fact that most surfaces are not simple structures and that surface layers could lead to significant effects.

13. APPENDIX B: SAMPLE ROTATION

The text considers the case in which the direction of the surface lay (tool marks) is perpendicular to the direction of the profile measurement. If the sample is rotated through an angle θ away from that direction, a given surface wavelength d appears at the longer wavelength:

$$d(\theta,R) = +[(R + d)^2 - (R\sin\theta)^2]^{1/2} - R\cos\theta , \tag{24}$$

where R is the machining radius. In the limit of large R/d,

$$d(\theta,R) = \frac{d}{\cos\theta} , \tag{25}$$

which is valid for all rotation angles except those very near 90°. In this way the apparent wavelength can easily be stretched by a factor of 10 (rotation of 84.3°).

The transfer function of the optical gauge is (presumably) circularly symmetric and therefore independent of the sample rotation. That is, the frequency appearing in Eq. (13) is the true surface frequency $f = 1/d$ rather than the apparent value given by Eqs. (24) or (25). However, since that transfer function vanishes for wavelengths less than 1 μm for the 20× instrument, the present stretching technique cannot give useful information about surface wavelengths shorter than that value.

The transfer function of the array does depend on the angle of rotation since its pixels are not circularly symmetric. As discussed in the text, the pixels are essentially squares that are summed pairwise to give a rectangular form with an aspect ratio of A = 2. That quantity appears as a factor in the common argument in the numerator and denominator of Eq. (15). In the case of a rotated sample, that factor A must be replaced by $A[\cos\theta + A\sin\theta]^{-1}$.

Sample rotation is useful for zooming in on high-frequency profile features (such as the fine structure of the 3.4 μm lines in the silicon surface), for examining wavelength contributions lying between the 1 μm microscope cutoff and the 2 μm filter cutoff, and for identifying aliased lines in the spectrum since they will move to higher rather than to lower frequencies as the sample is rotated from $\theta = 0$.

14. REFERENCES

1. E. L. Church, in *Precision Surface Metrology,* James C. Wyant, ed., Proc. SPIE 429, 105 (1983).
2. E. C. Teague, Nat. Bur. Stand. (U.S.) Technical Note 902 (1976).
3. T. V. Vorburger, E. C. Teague, and F. E. Scire, Dimensions/NBS 62(11), 18 (1978).
4. J. C. Wyant, C. L. Koliopolis, B. Bhushan, and O. E. George, Am. Soc. Lub. Engrs. Trans. 27, 101 (1984).
5. E. L. Church, M. R. Howells, and T. V. Vorburger, in *Reflecting Optics for Synchrotron Radiation,* Malcom R. Howells, ed., Proc. SPIE 315, 202 (1982).
6. E. L. Church and H. C. Berry, Wear 83, 189 (1982).
7. E. L. Church, in *Precision Surface Metrology,* James C. Wyant, ed., Proc. SPIE 429, 86 (1983).
8. E. L. Church, H. A. Jenkinson, and J. M. Zavada, Opt. Eng. 16(4), 360 (1977).
9. E. L. Church and P. Z. Takacs, Opt. Eng. 24(3), (1985).
10. E. L. O'Neill, J. Opt. Soc. Am. 46, 285 (1956).